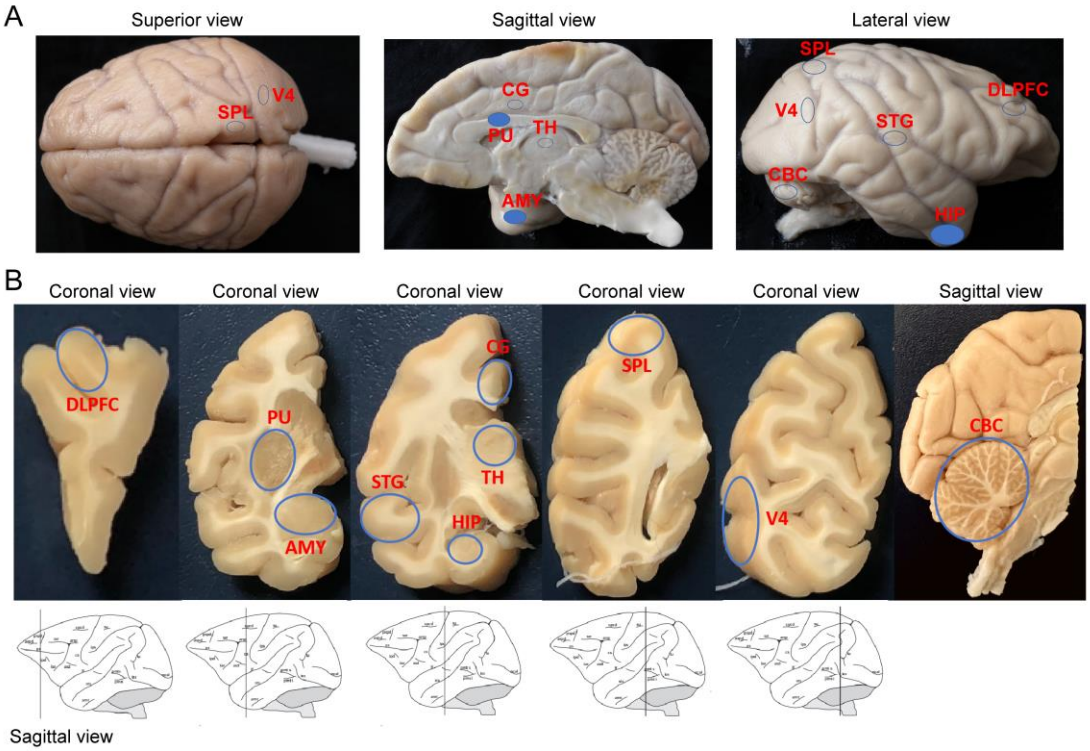

Fig. S1. Anatomy of the ten dissected brain regions used for snRNA-seq in rhesus macaque. (A) Superior, sagittal and lateral views for the ten brain regions. Ellipses filled by blue represent the regions being collected inside this area. (B) Coronal and sagittal views of the ten brain regions used for histological verification. AMY: amygdala; PU: putamen; HIP: hippocampus; TH: thalamus; DLPFC: dorsolateral prefrontal cortex; CG: cingulate gyrus; STG: superior temporal gyrus; SPL: superior parietal lobule; V4: visual cortex V4; CBC: cerebellar cortex.

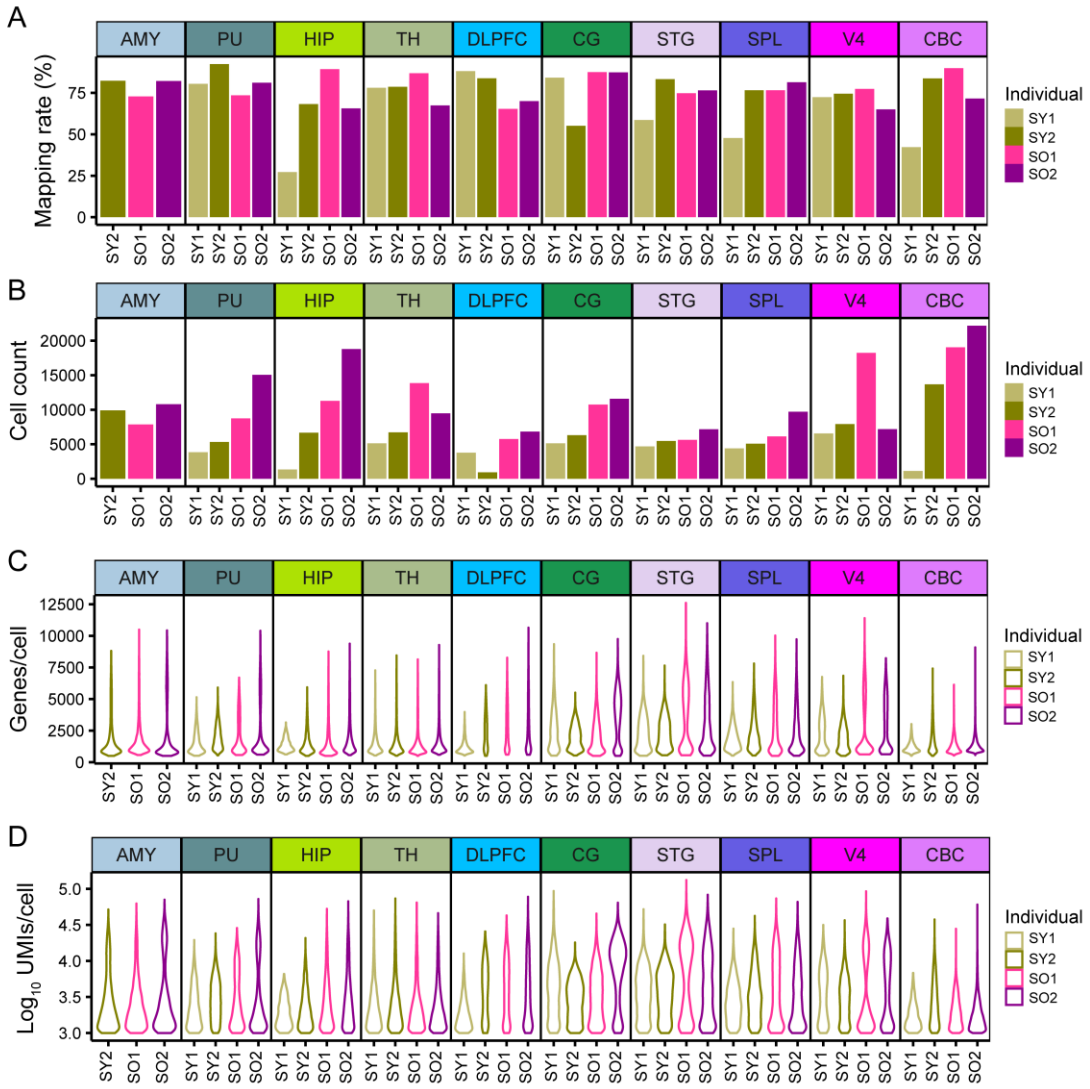

Fig. S2. Statistical information summarizing the data across the 39 brain samples. (A) Genome mapping rate of uniquely mapped reads for each sample. (B) Number of nuclei obtained in each sample. (C) Violin plot shows number of genes expressed in a cell for each sample. (D) Violin plot displays number of log-transformed UMIs observed in a cell for each sample.

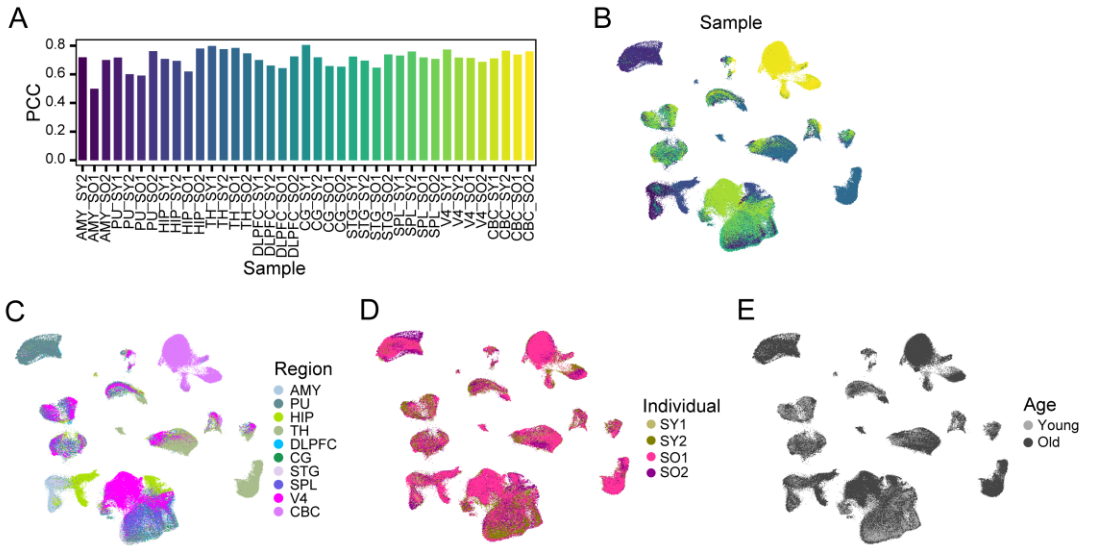

Fig. S3. Characterization of consistent expression profiles. (A) Correlation of gene expression ascertained from snRNA-seq data and their corresponding bulk RNA-seq data. PCC: Pearson correlation coefficient. (B–E) Uniform Manifold Approximation and Projection (UMAP) plots show good integration of nuclei across the 39 samples (B), 10 brain regions (C), 4 individuals (D), 2 age groups (E). The sample colors in (B) are the same as in (A).

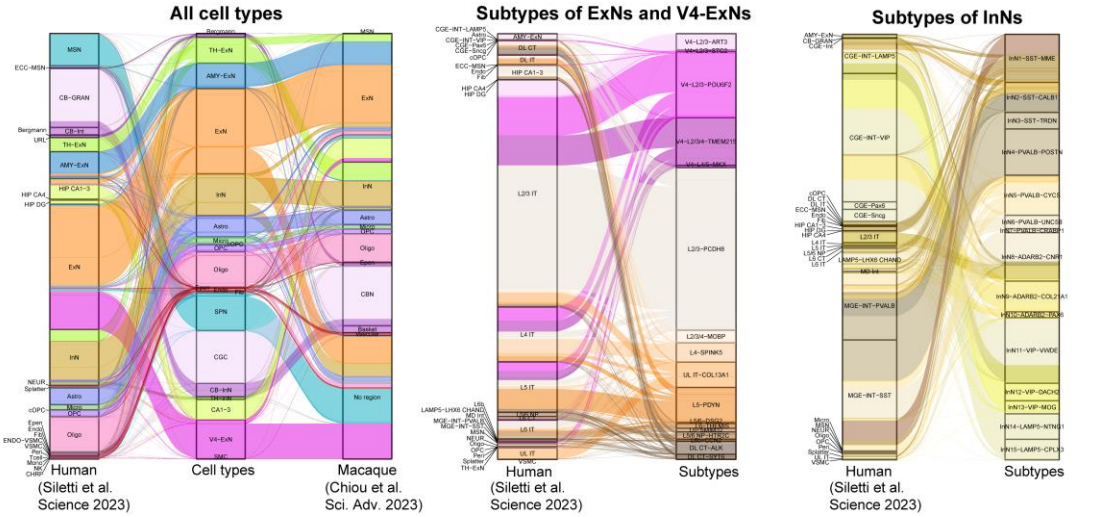

Fig. S4. Comparisons of our cell annotation with published NHP brain snRNA-seq datasets. Alluvial plots show the number of our nuclei transferred to the two published NHP brain snRNA-seq datasets. From left to right: the nuclei number of the twenty major cell types transferred to the cell types from the published human and macaque datasets (first); the nuclei number of subtypes of cortical excitatory neurons (ExNs) transferred to human excitatory subtypes (second); the nuclei number of subtypes of inhibitory neurons (InNs) transferred to human inhibitory subtypes

(third). “No region” means the published macaque dataset lacked some regions with same anatomical origins to our regions. Meanwhile, the published macaque dataset had no subtypes of ExNs and InNs, thus only the human dataset was used for excitatory and inhibitory subtypes transferring. SPN: spiny projection neuron; CGC: cerebellar granule cell; CB-InN: InN mainly from CBC; TH-ExN: ExN mainly from TH; TH-InN: InN mainly from TH; AMY-ExN: ExN mainly from AMY; CA1–3: hippocampal excitatory CA1–3 cell; V4-ExN: ExN mainly from V4; Astro: astrocyte; Micro: microglia; OPC: oligodendrocyte progenitor cell; cOPC: differentiation committed OPC; Oligo: oligodendrocyte; Epen: ependymal cell; Endo: endothelial cell; Fib: perivascular fibroblast; SMC: smooth muscle cell; L5/6 NP: L5-6 near-projecting ExN; UL IT: upper-layer intratelencephalic-projecting ExN; DL CT: deep-layer corticothalamic-projecting ExN.

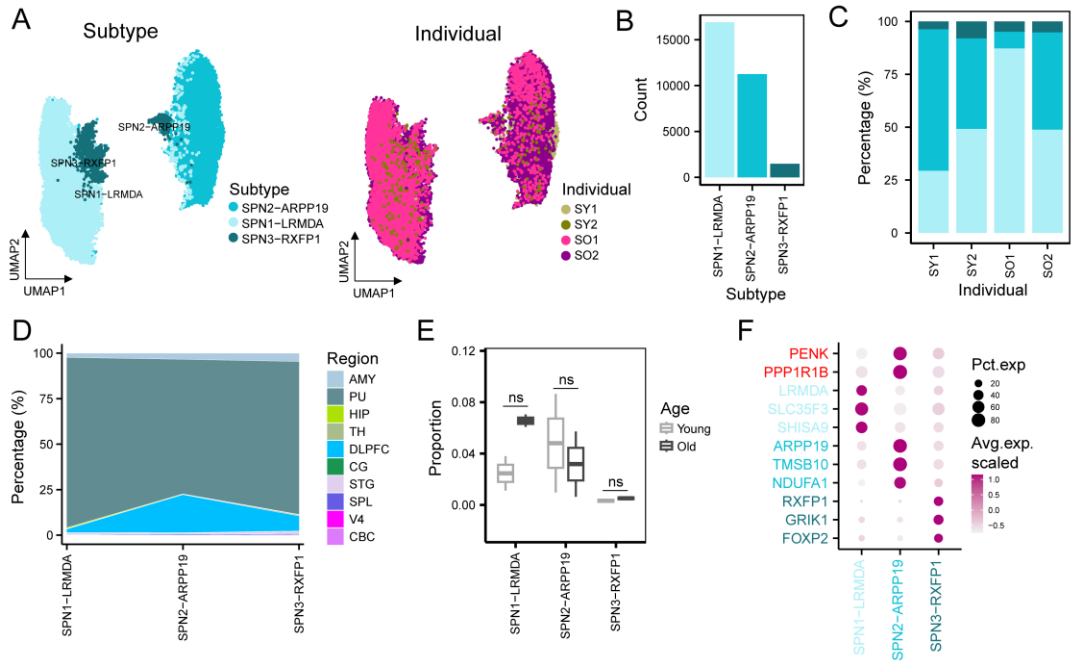

Fig. S5. Subtype features of the putamen-specific group (i.e., SPNs). (A) UMAP plot of nuclei clustered into 3 subtypes (left) or across 4 individuals (right). (B) Number of nuclei in each subtype. (C) Percentage of nuclei across subtypes for each individual. (D) Percentage of nuclei across brain regions for each subtype. (E) Box plot of nuclei proportion across the two age groups for each subtype. *: $P<0.05$; ns: $P>0.05$, using a linear regression model with sex as a covariate. Gray * represents proportion of the subtype significant lower in the old group, while black * is the opposite. (F) Dot plot shows the expression of subtype marker genes. The dot size represents the percentage of nuclei expressing a gene in a given subtype, whereas dot color represents the average expression level. Well-known SPN markers were colored by red.

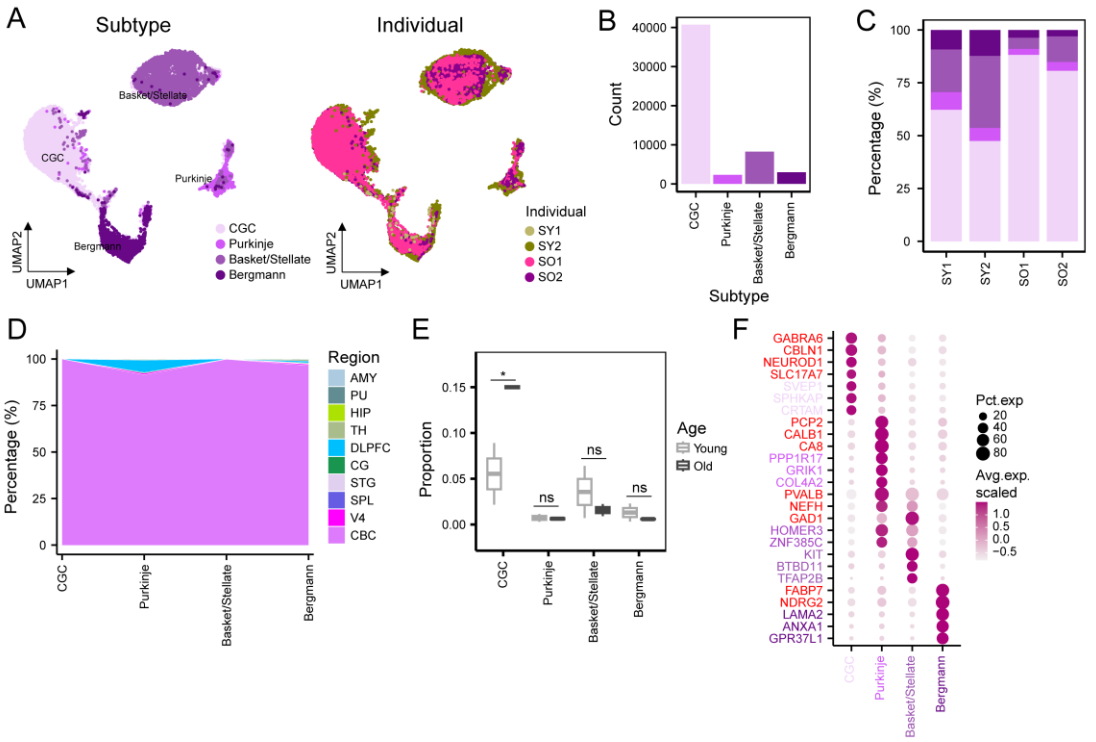

Fig. S6. Subtype features of the cerebellum-specific group (i.e., CGCs, CB-InNs and Bergmanns). (A) UMAP plot of nuclei with CB-InNs being clustered into 2 subtypes (left) or across 4 individuals (right). (B) Number of nuclei in each subtype. (C) Percentage of nuclei across subtypes for each individual. (D) Percentage of nuclei across brain regions for each subtype. (E) Box plot of nuclei proportion across the two age groups for each subtype. *: $P<0.05$; ns: $P>0.05$, using a linear regression model with sex as a covariate. Gray * represents proportion of the subtype significant lower in the old group, while black * is the opposite. (F) Dot plot shows the expression of subtype marker genes. The dot size represents the percentage of nuclei expressing a gene in a given subtype, whereas dot color represents the average expression level. Well-known markers of CGCs, Purkinje neurons, basket/stellate cells and Bergmanns were colored by red.

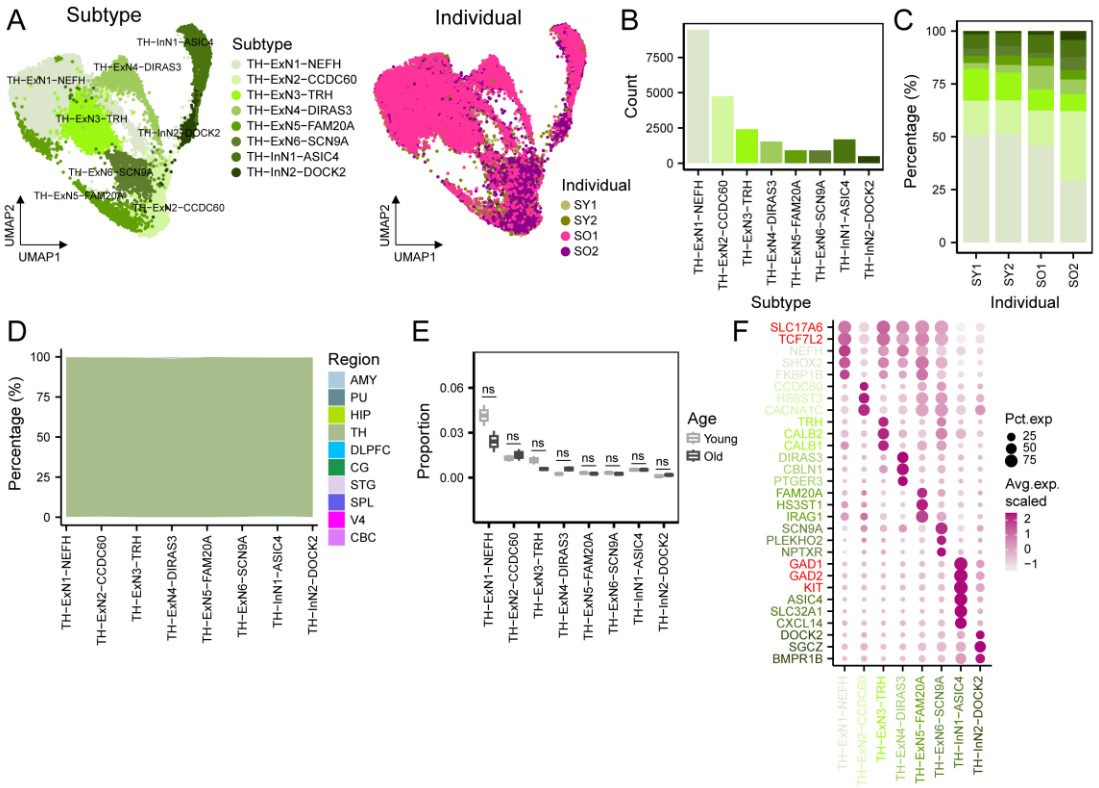

Fig. S7. Subtype features of the thalamus-specific group (i.e., TH-ExNs and TH-InNs). (A) UMAP plot of nuclei clustered into 8 subtypes (left) or across 4 individuals (right). (B) Number of nuclei in each subtype. (C) Percentage of nuclei across subtypes for each individual. (D) Percentage of nuclei across brain regions for each subtype. (E) Box plot of nuclei proportion across the two age groups for each subtype. *: $P<0.05$; ns: $P>0.05$, using a linear regression model with sex as a covariate. Gray * represents proportion of the subtype significant lower in the old group, while black * is the opposite. (F) Dot plot shows the expression of subtype marker genes. The dot size represents the percentage of nuclei expressing a gene in a given subtype, whereas dot color represents the average expression level. Well-known markers of TH-ExNs and TH-InNs were colored by red.

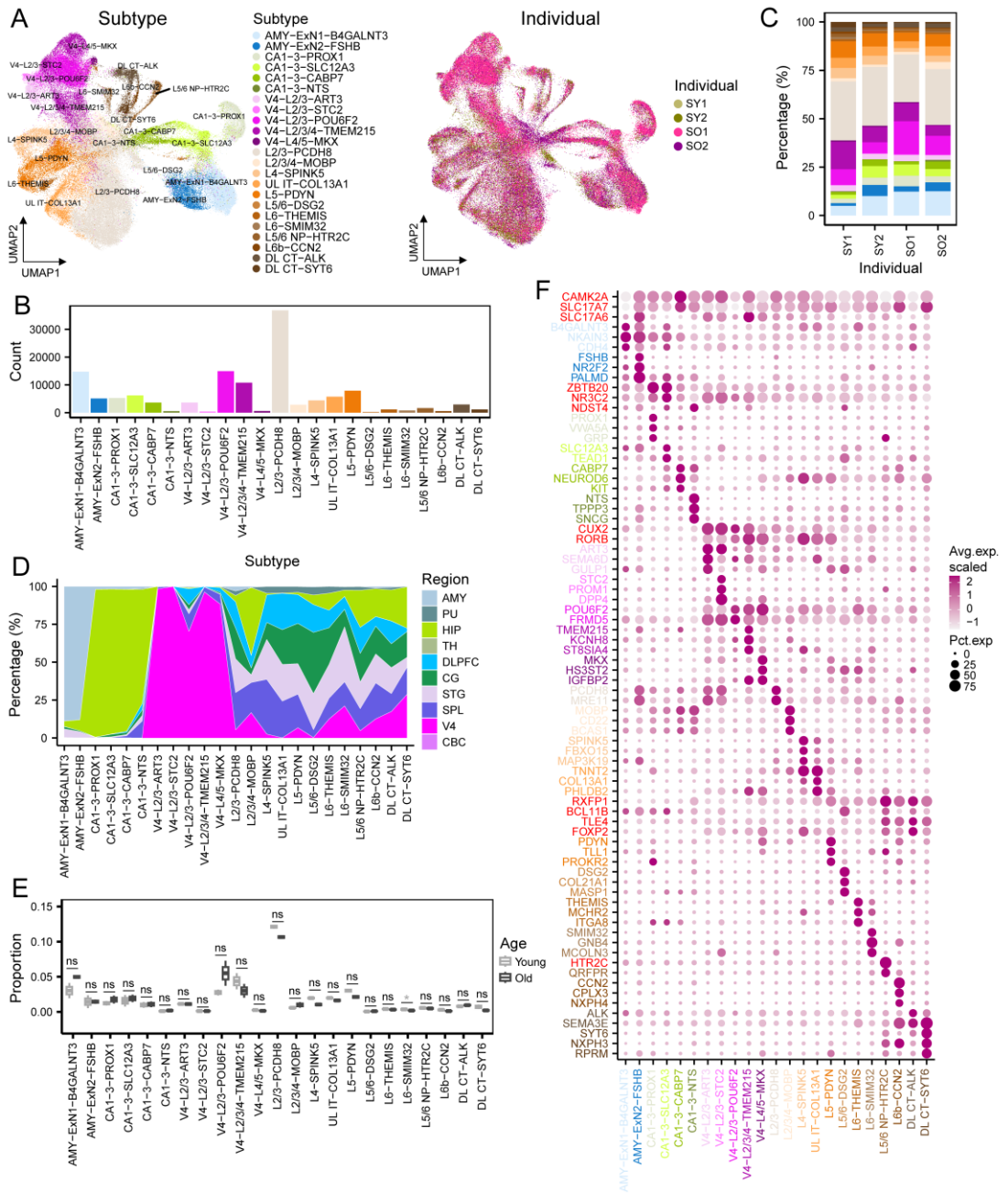

Fig. S8. Subtype features of the excitatory group (i.e., AMY-ExNs, CA1–3s, V4-ExNs and ExNs). (A) UMAP plot of nuclei clustered into 23 subtypes (left) or across 4 individuals (right). (B) Number of nuclei in each subtype. (C) Percentage of nuclei across subtypes for each individual. (D) Percentage of nuclei across brain regions for each subtype. (E) Box plot of nuclei proportion across the two age groups for each subtype. *: P<0.05; ns: P>0.05, using a linear regression model with sex as a covariate. Gray * represents proportion of the subtype significant lower in the old group, while black * is the opposite. (F) Dot plot shows the expression of subtype marker genes. The dot size represents the percentage of nuclei expressing a gene in a given subtype, whereas dot color represents the average expression level. Well-known markers of AMY-ExNs, CA1–3s and cortical layers were colored by red.

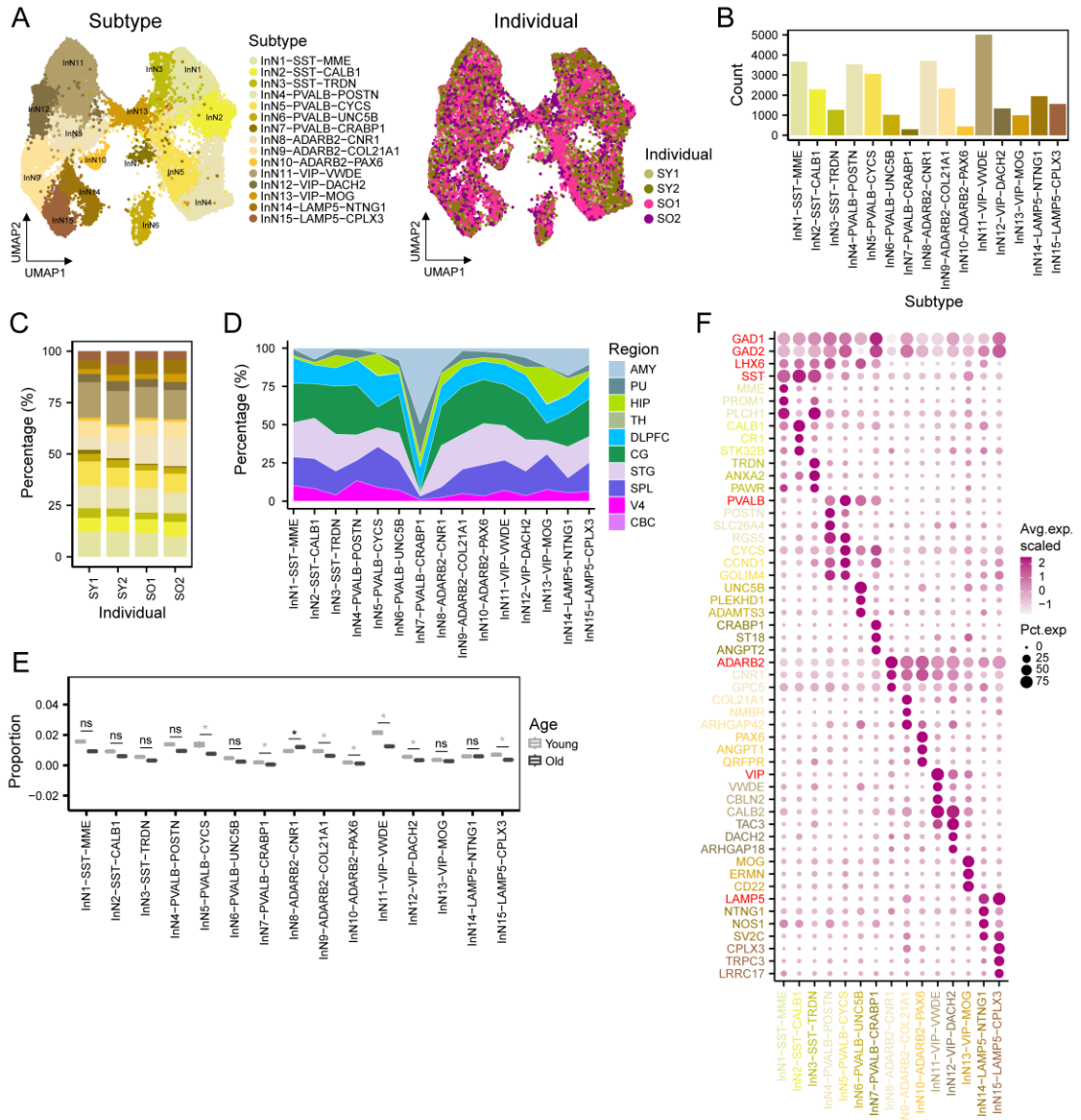

Fig. S9. Subtype features of the inhibitory group (i.e., InNs). (A) UMAP plot of nuclei clustered into 15 subtypes (left) or across 4 individuals (right). (B) Number of nuclei in each subtype. (C) Percentage of nuclei across subtypes for each individual. (D) Percentage of nuclei across brain regions for each subtype. (E) Box plot of nuclei proportion across the two age groups for each subtype. *: P<0.05; ns: P>0.05, using a linear regression model with sex as a covariate. Gray * represents proportion of the subtype significant lower in the old group, while black * is the opposite. (F) Dot plot shows the expression of subtype marker genes. The dot size represents the percentage of nuclei expressing a gene in a given subtype, whereas dot color represents the average expression level. Well-known markers of InNs and its subtypes were colored by red.

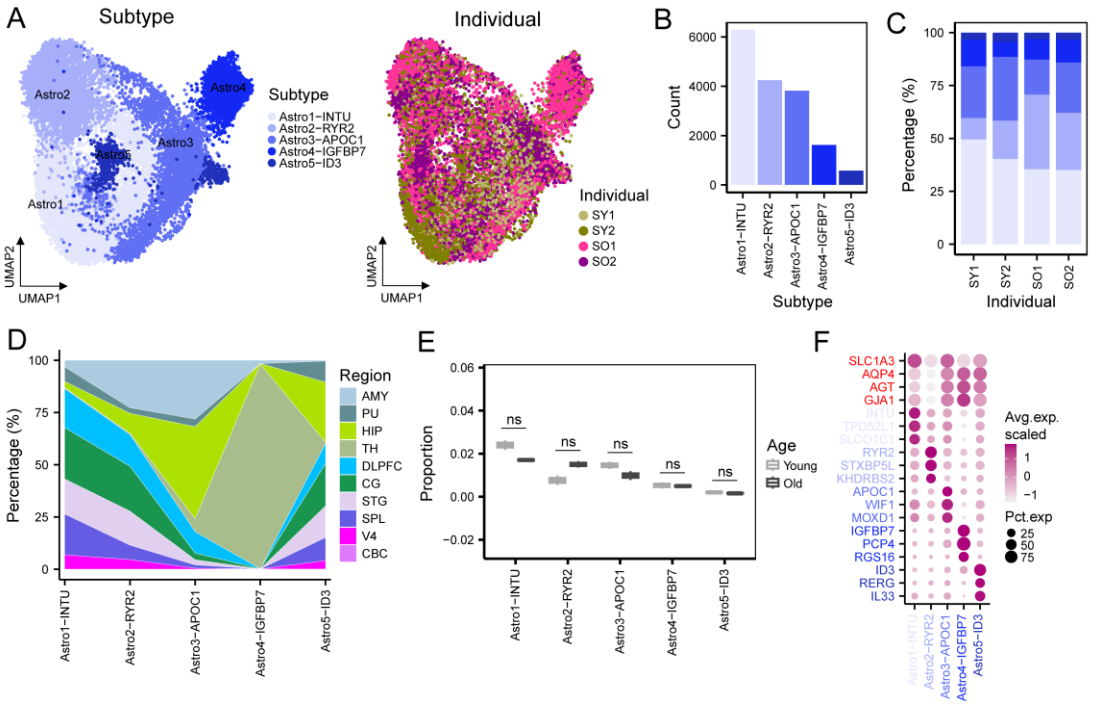

Fig. S10. Subtype features of the astrocytic group (i.e., Astros). (A) UMAP plot of nuclei clustered into 5 subtypes (left) or across 4 individuals (right). (B) Number of nuclei in each subtype. (C) Percentage of nuclei across subtypes for each individual. (D) Percentage of nuclei across brain regions for each subtype. (E) Box plot of nuclei proportion across the two age groups for each subtype. *: $P<0.05$; ns: $P>0.05$, using a linear regression model with sex as a covariate. Gray * represents proportion of the subtype significant lower in the old group, while black * is the opposite. (F) Dot plot shows the expression of subtype marker genes. The dot size represents the percentage of nuclei expressing a gene in a given subtype, whereas dot color represents the average expression level. Well-known markers of Astros were colored by red.

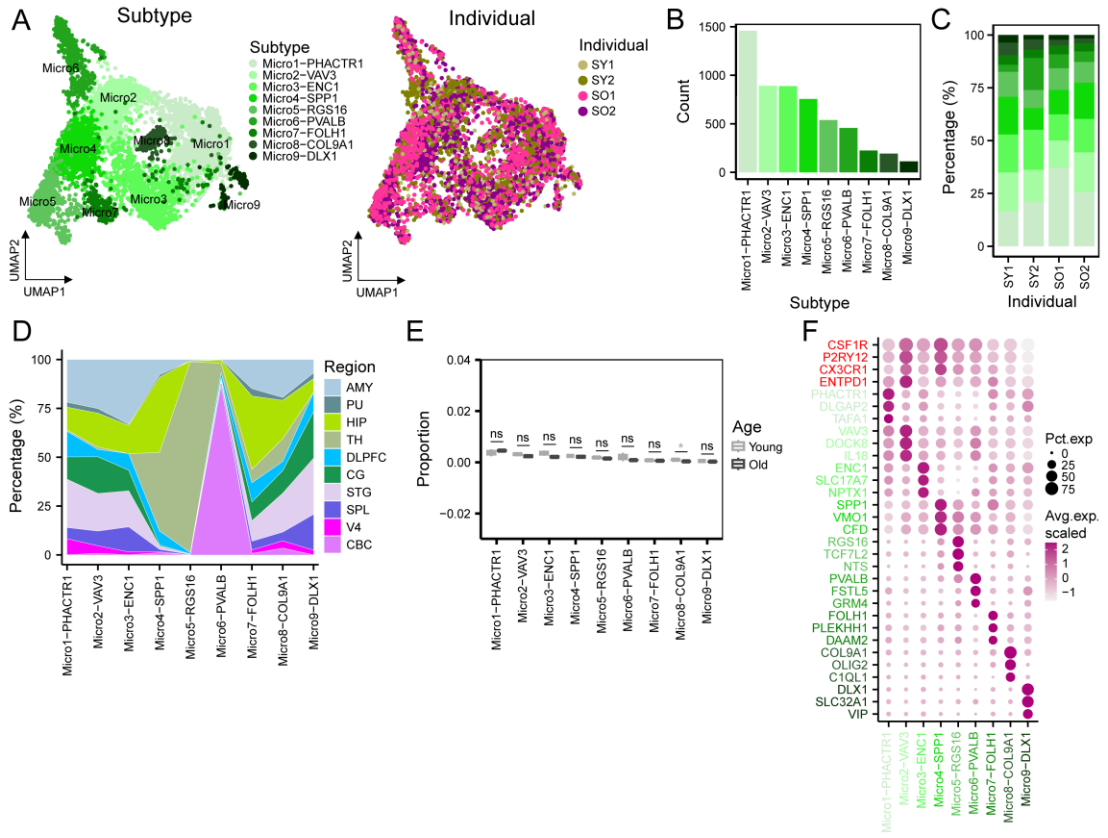

Fig. S11. Subtype features of the microglial group (i.e., Micros). (A) UMAP plot of nuclei clustered into 9 subtypes (left) or across 4 individuals (right). (B) Number of nuclei in each subtype. (C) Percentage of nuclei across subtypes for each individual. (D) Percentage of nuclei across brain regions for each subtype. (E) Box plot of nuclei proportion across the two age groups for each subtype. *: P<0.05; ns: P>0.05, using a linear regression model with sex as a covariate. Gray * represents proportion of the subtype significant lower in the old group, while black * is the opposite. (F) Dot plot shows the expression of subtype marker genes. The dot size represents the percentage of nuclei expressing a gene in a given subtype, whereas dot color represents the average expression level. Well-known markers of Micros were colored by red.

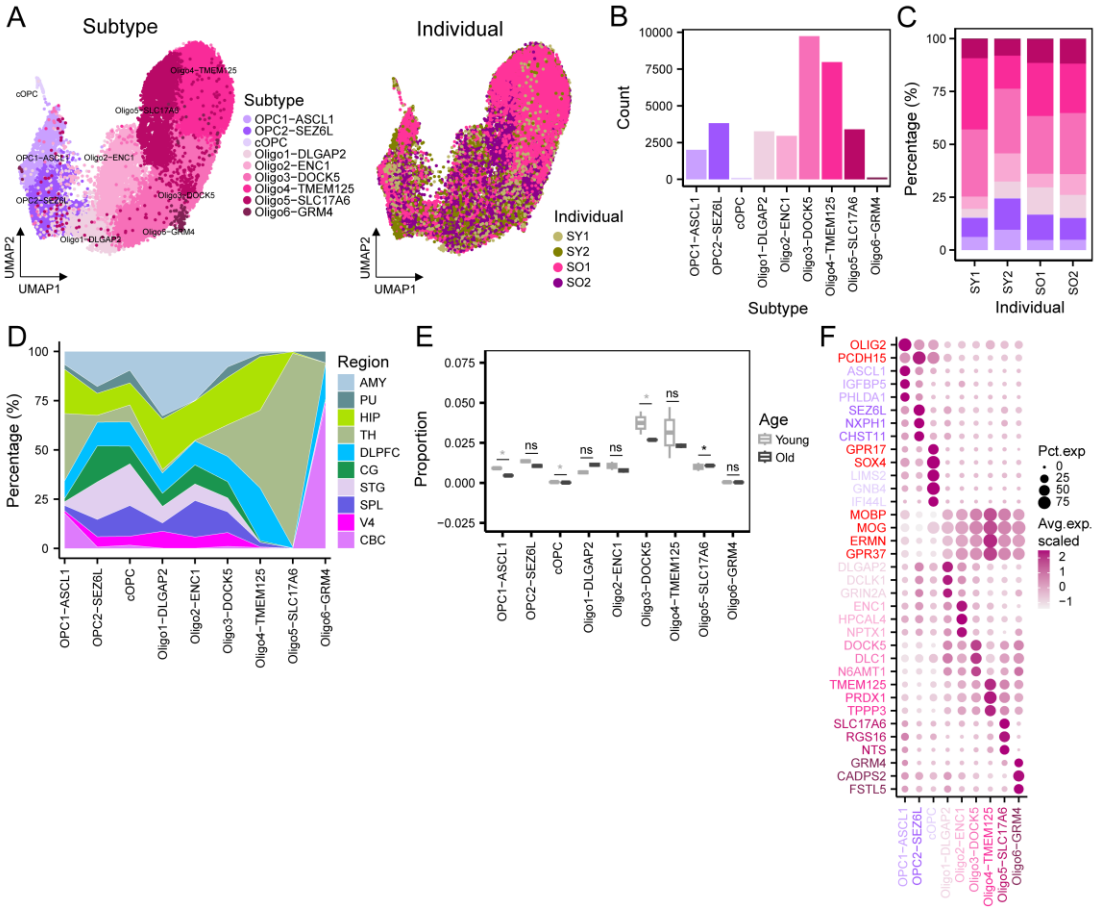

Fig. S12. Subtype features of the oligodendrocyte-lineage group (i.e., OPCs, cOPCs and Oligos). (A) UMAP plot of nuclei with OPCs and Oligos being clustered into 2 and 6 subtypes, respectively (left), or nuclei across 4 individuals (right). (B) Number of nuclei in each subtype. (C) Percentage of nuclei across subtypes for each individual. (D) Percentage of nuclei across brain regions for each subtype. (E) Box plot of nuclei proportion across the two age groups for each subtype. *: $P<0.05$; ns: $P>0.05$, using a linear regression model with sex as a covariate. Gray * represents proportion of the subtype significant lower in the old group, while black * is the opposite. (F) Dot plot shows the expression of subtype marker genes. The dot size represents the percentage of nuclei expressing a gene in a given subtype, whereas dot color represents the average expression level. Well-known markers of OPCs, cOPCs and Oligos were colored by red.

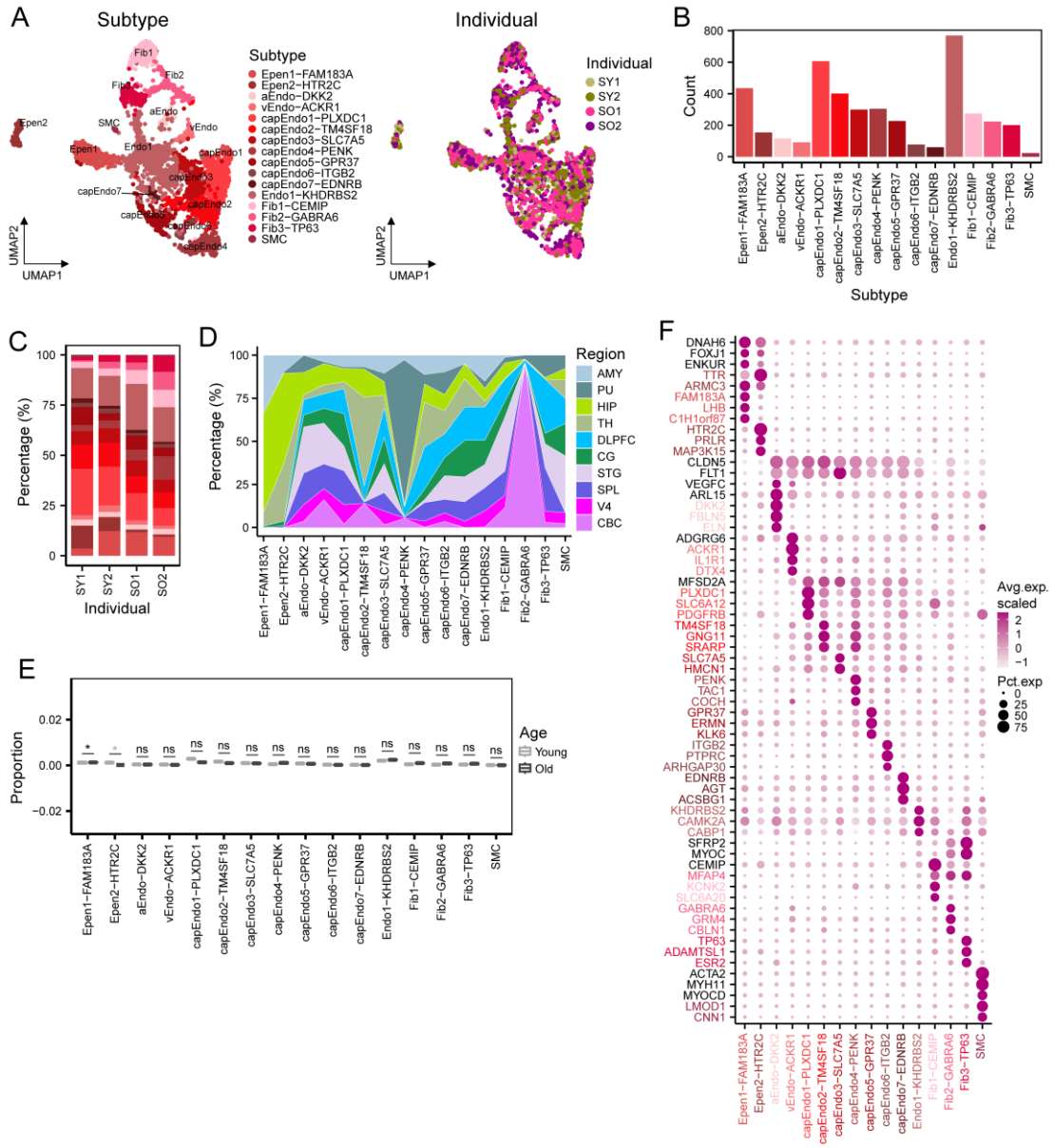

Fig. S13. Subtype features of the membrane-related non-neuronal cell type group (i.e., Epens, Endos, Fibs and SMCs). (A) UMAP plot of nuclei with Epens, Endos and Fibs being clustered into 2, 10 and 3 subtypes, respectively (left), or nuclei across 4 individuals (right). (B) Number of nuclei in each subtype. (C) Percentage of nuclei across subtypes for each individual. (D) Percentage of nuclei across brain regions for each subtype. (E) Box plot of nuclei proportion across the two age groups for each subtype. *: P<0.05; ns: P>0.05, using a linear regression model with sex as a covariate. Gray * represents proportion of the subtype significant lower in the old group, while black * is the opposite. (F) Dot plot shows the expression of subtype marker genes. The dot size represents the percentage of nuclei expressing a gene in a given subtype, whereas dot color represents the average expression level. Well-known markers of Epens, Endos, Fibs and SMCs were colored by black. aEndos: arteriole Endos; vEndos: venule Endos; capEndos: capillary Endos.

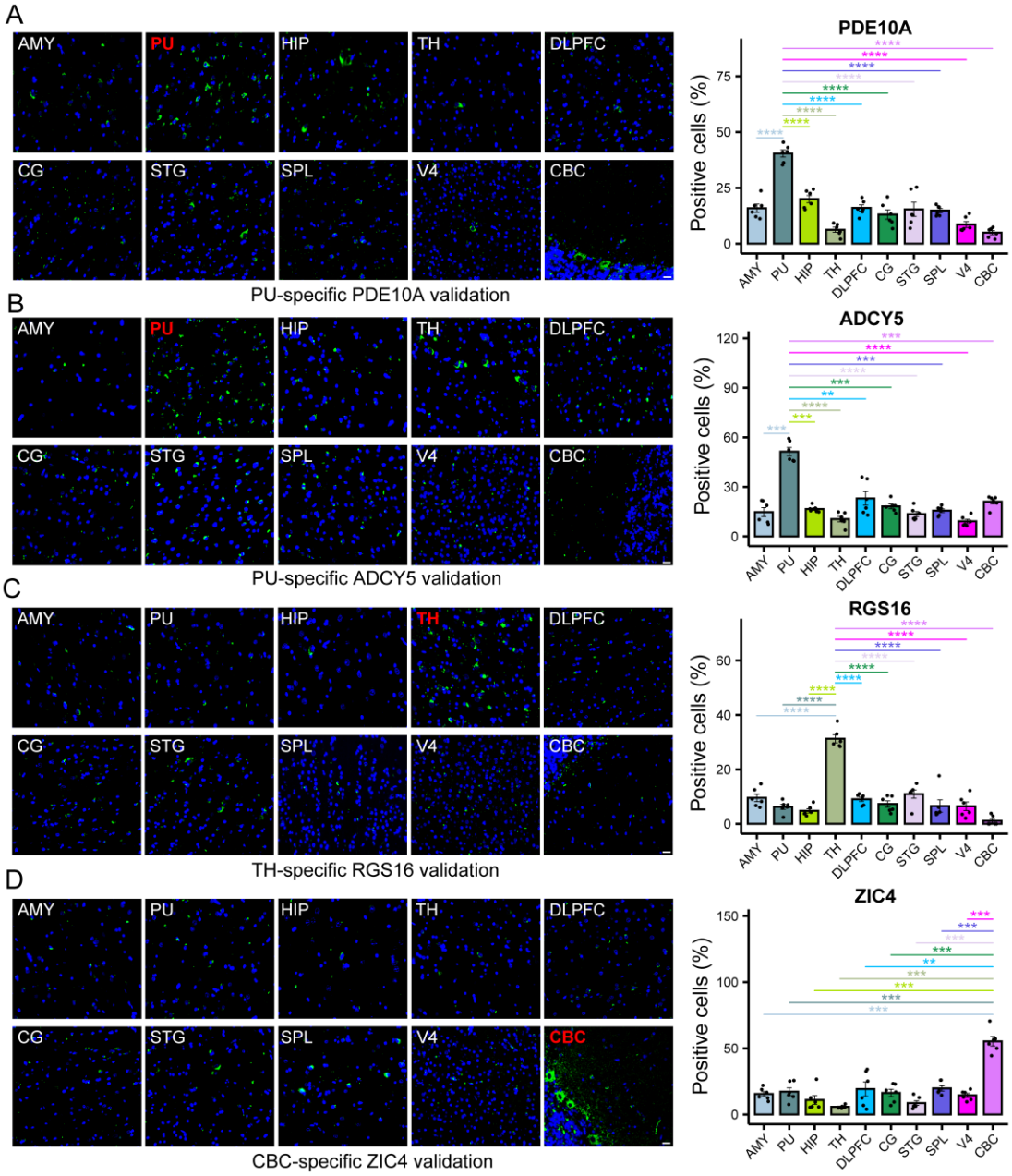

Fig. S14. Validation of protein expression across the ten brain regions of interest for the selected region-specific genes (RSGs). (A–D) Immunofluorescence validation of RSG protein expression across the ten regions, including PDE10A for PU (A), ADCY5 for PU (B), RGS16 for TH (C), ZIC4 for CBC (D). Bar plots (right) represent the mean percentage of immunopositive cells for each staining across three visual fields with standard error of mean bars. One-way ANOVA was applied for PDE10A and RGS16 followed by Dunnett multiple comparisons due to normal distribution and equal variances, while Welch's ANOVA was applied for ADCY5 and ZIC4 followed by Games-Howell test and adjusting *P* values using FDR due to normal distribution but unequal variances. ****: adjusted *P* value (P_{adj}) <0.0001; ***: P_{adj}<0.001; **: P_{adj}<0.01; *: P_{adj}<0.05. Scale bars: 20 μm.

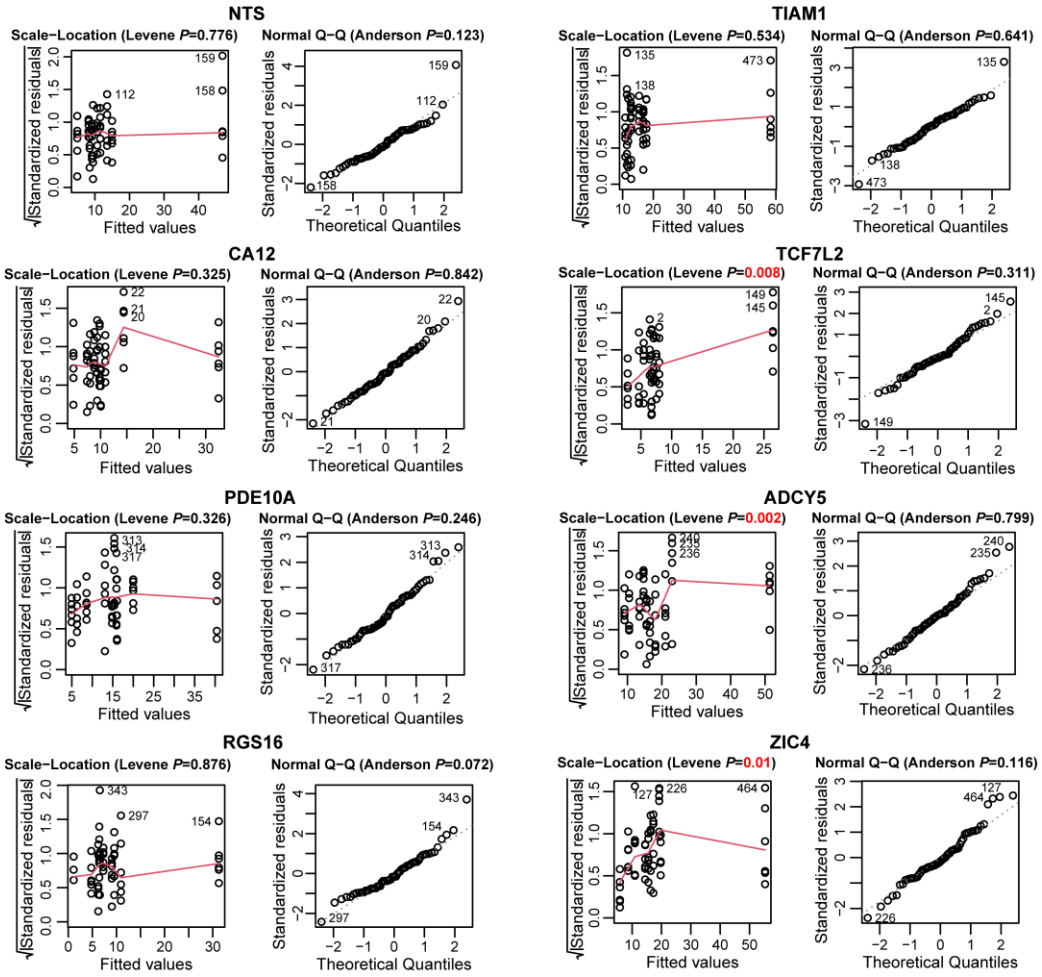

Fig. S15. Examination of data distributions of the selected RSGs from immunofluorescence staining. For each RSG, the first panel from left to right: scale-location plot for homogeneity of variances with Levene's test *P* value being shown; the second panel: Q-Q plot of residuals versus fitted values for normality with Anderson-Darling test *P* value being shown. *P* values <0.05 were marked by red to represent unequal variances from Levene's test or abnormal distribution from Anderson-Darling test.

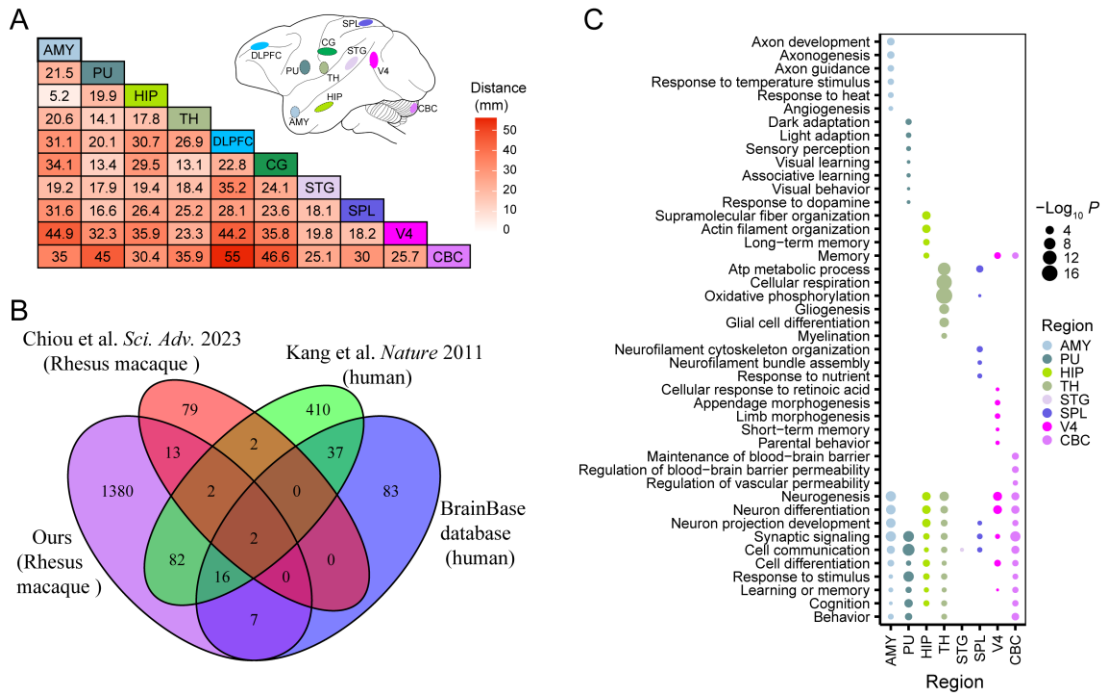

Fig. S16. Transcriptomic features across brain regions. (A) Heat map depicts spatial distance values between any two of the ten brain regions. (B) Venn diagram indicates the number of intersected region-specific genes (RSGs) identified by our and other three published NHP datasets. (C) Significant annotation categories of RSGs. Dot size represents −log-transformed *P* values and their color is the same as the regional color.

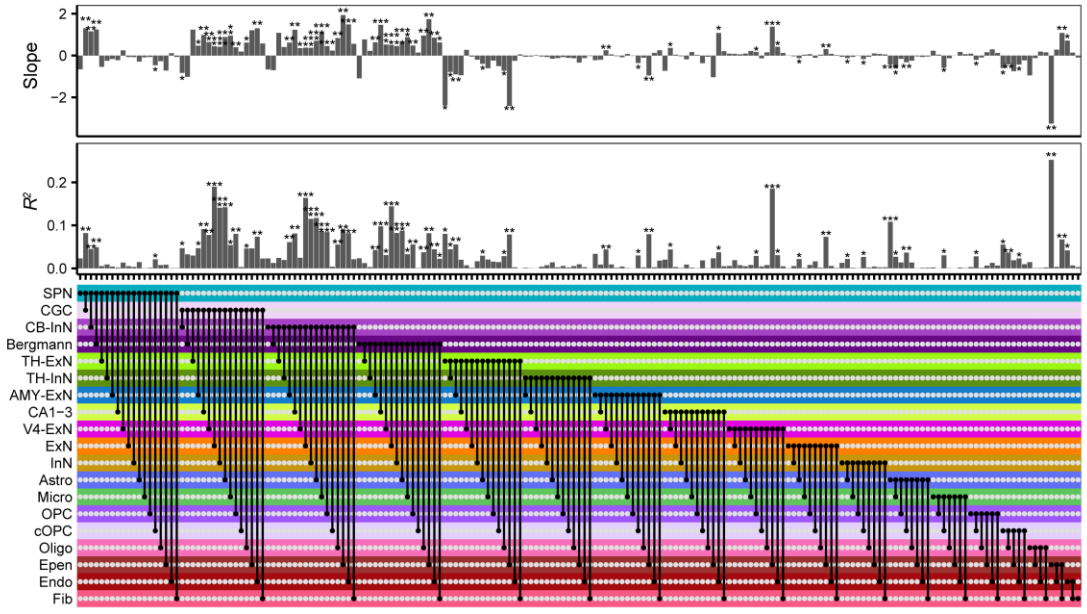

Fig. S17. Correlations between intra- or inter-region cellular communication and spatial distance. Slope, R^2 and *P* values were calculated using "lm". ***: $P<0.001$;

**: P<0.01; *: P<0.05.

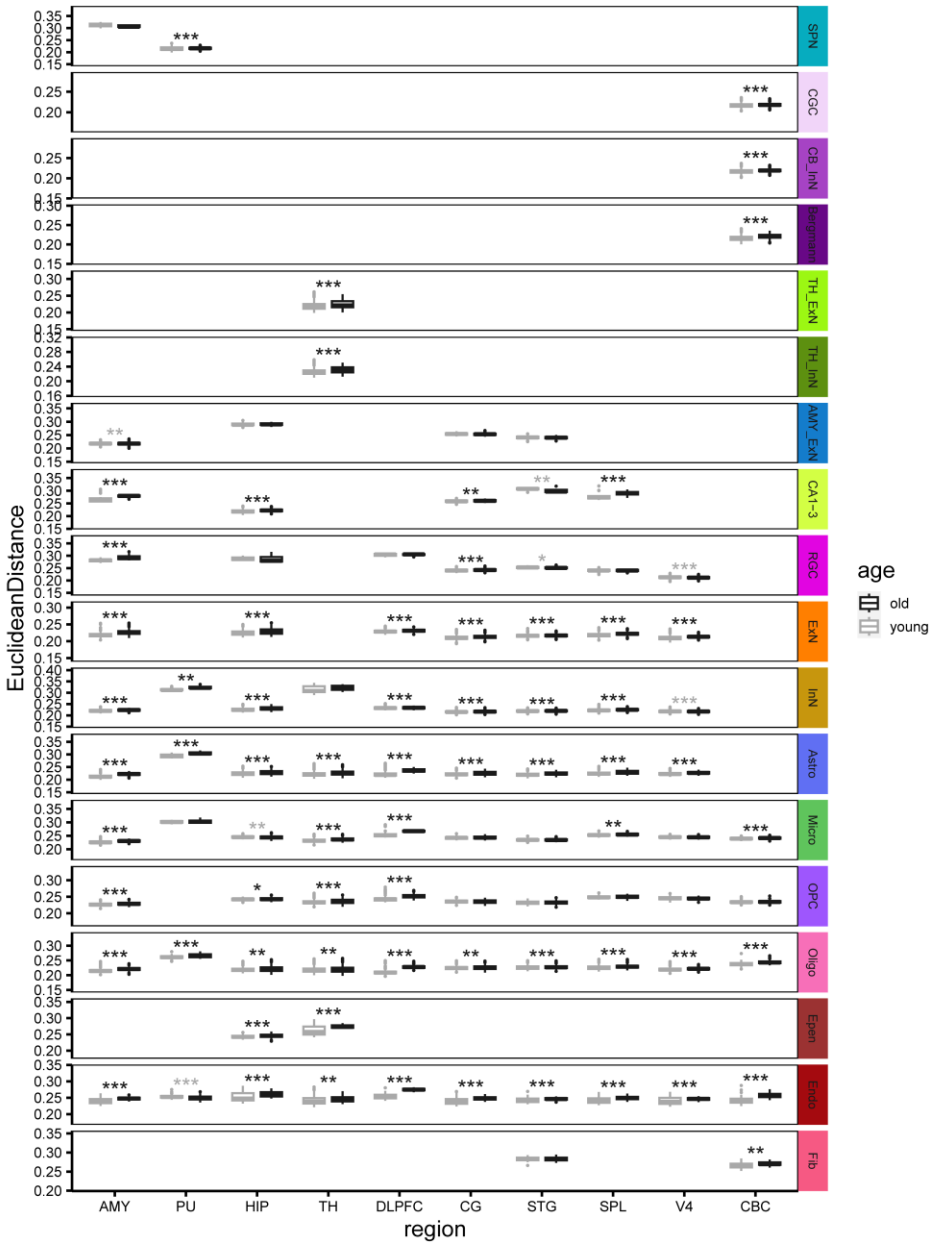

Fig. S18. Boxplot indicates comparison of transcriptional noise across different cell types and brain regions between young and old individuals. ***: P<0.001; **: P<0.01; *: P<0.05, Wilcoxon rank-sum test. Light gray stars highlight significantly higher transcriptional noise in the young macaques than in the old, whereas black stars highlight significantly higher transcriptional noise in the old macaques than in the young.

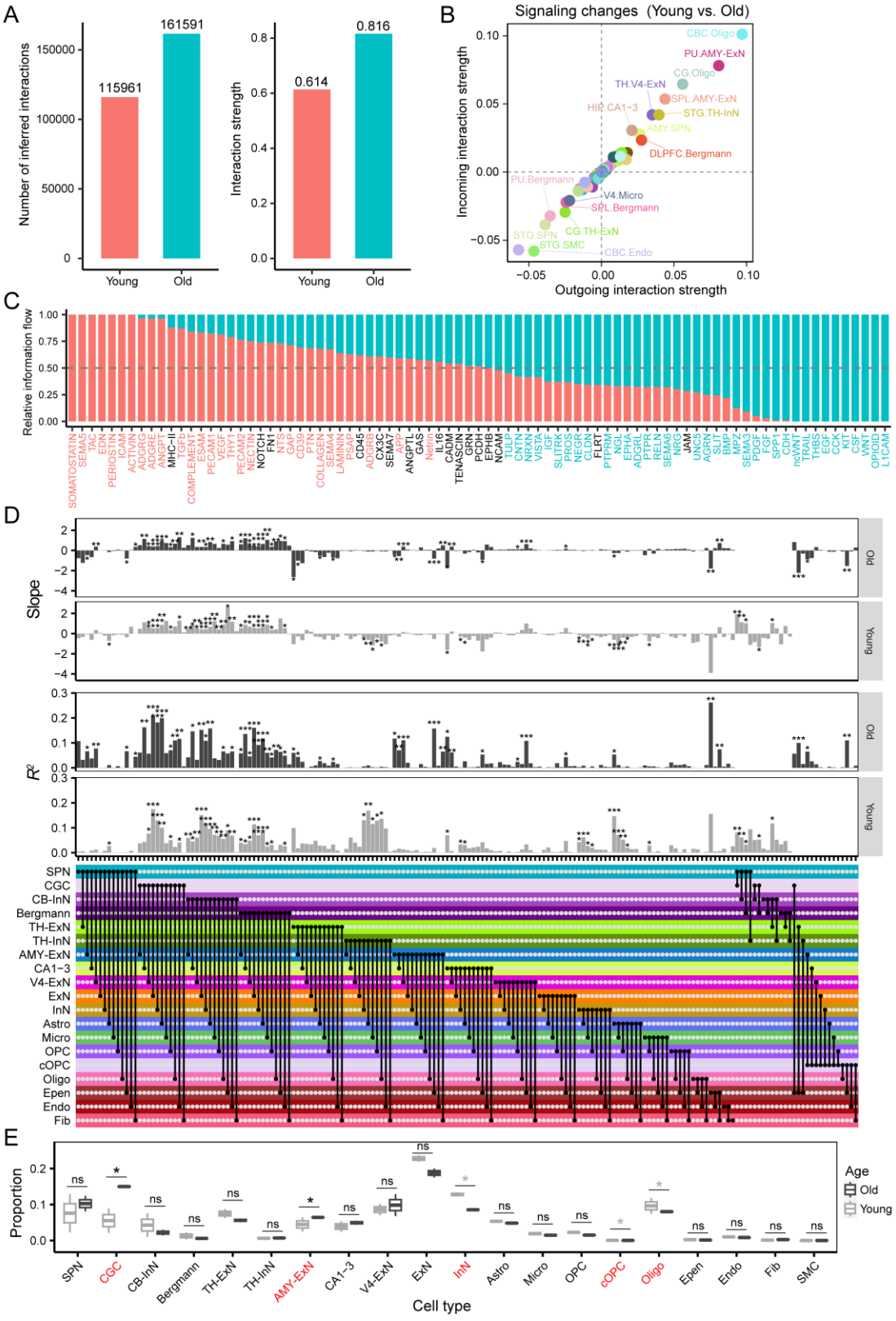

Fig. S19. Alterations in cellular communication with aging. (A) The number (left) and strength (right) of inferred interactions across cell types and regions for the young and old groups. (B) Signaling changes in sending or receiving signals for the major cell types across the ten brain regions between the young and old groups. Positive values in the differential outgoing (or incoming) interaction strength represent the

increased likelihood being sender (or receiver) in the old macaques compared to the young individuals. (C) Comparisons of signaling pathways based on the relative information flow between the young and old groups. Pathways enriched in the young group were colored by red, while those enriched in the old group were colored by green. (D) Correlations of intra- or inter-region cellular communication and spatial distance for the young and old macaques, respectively. Slope, R^2 and P values were calculated using "lm". ***: P<0.001; **: P<0.01; *: P<0.05. (E) Box plot of nuclei proportion across cell types for the two age groups. *: P<0.05; ns: P>0.05, using a linear regression model with sex as a covariate. Gray * represents proportion of the cell type significant lower in the old group, while black * is the opposite, with their corresponding labels were colored by red.

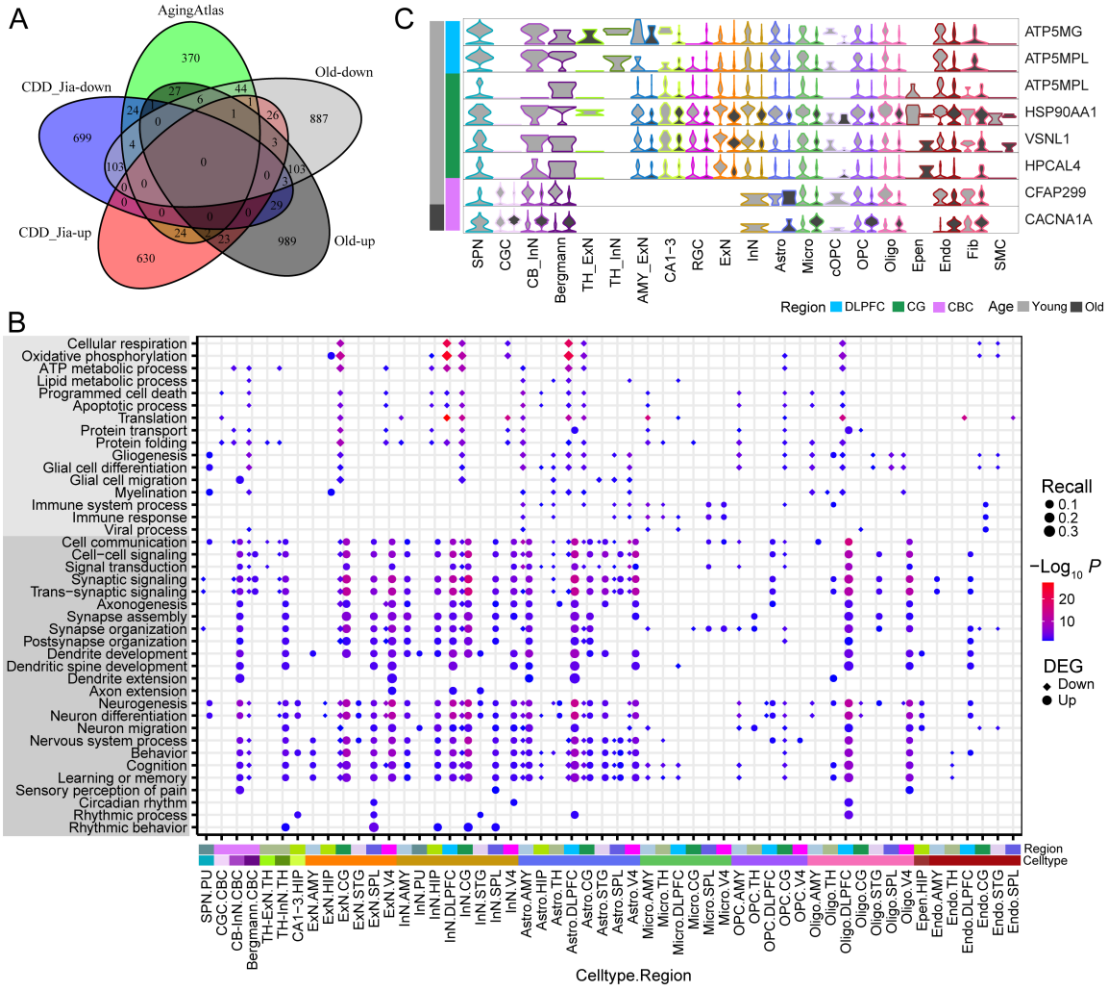

Fig. S20. Comparison of gene expression profiles between young and old macaque brains. (A) Venn diagram indicates the number of intersected aging-related genes identified by our and other two published human datasets. (B) Significant annotation categories of old-down-regulated (marked by Rhombi) or old-up-regulated (marked by circles) DEGs across cell types and regions. Dot size represents ratio of cell type markers in a term and their color is −log-transformed P values. (C) Violin

plot illustrates expression of differentially expressed genes (DEGs) validated by immunohistochemistry staining across cell types in the corresponding brain regions between the young and old macaques. Border and inner colors of the violins correspond to the colors of the cell types and age groups, respectively.

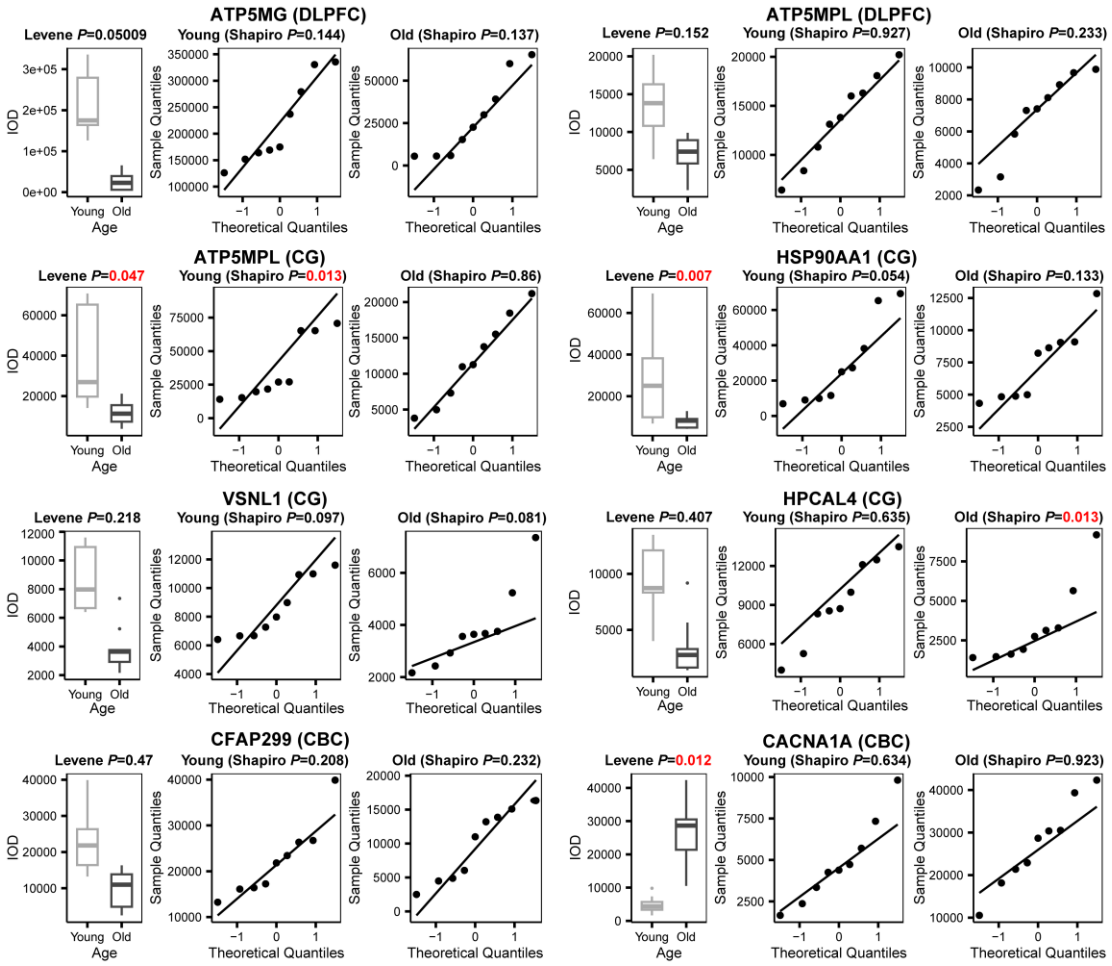

Fig. S21. Examination of data distributions of the selected aging-related genes from immunohistochemical staining. For each gene, the first panel from left to right: box plot of the mean integrated optical density (IOD) for checking homogeneity of variances with Levene's test *P* value being shown; the second and third panels: Q-Q plots of raw values versus theoretical values for normality with Shapiro-Wilk test *P* values being shown in the young and old groups, respectively. *P* values <0.05 were marked by red to represent unequal variances from Levene's test or abnormal distribution from Shapiro-Wilk test.

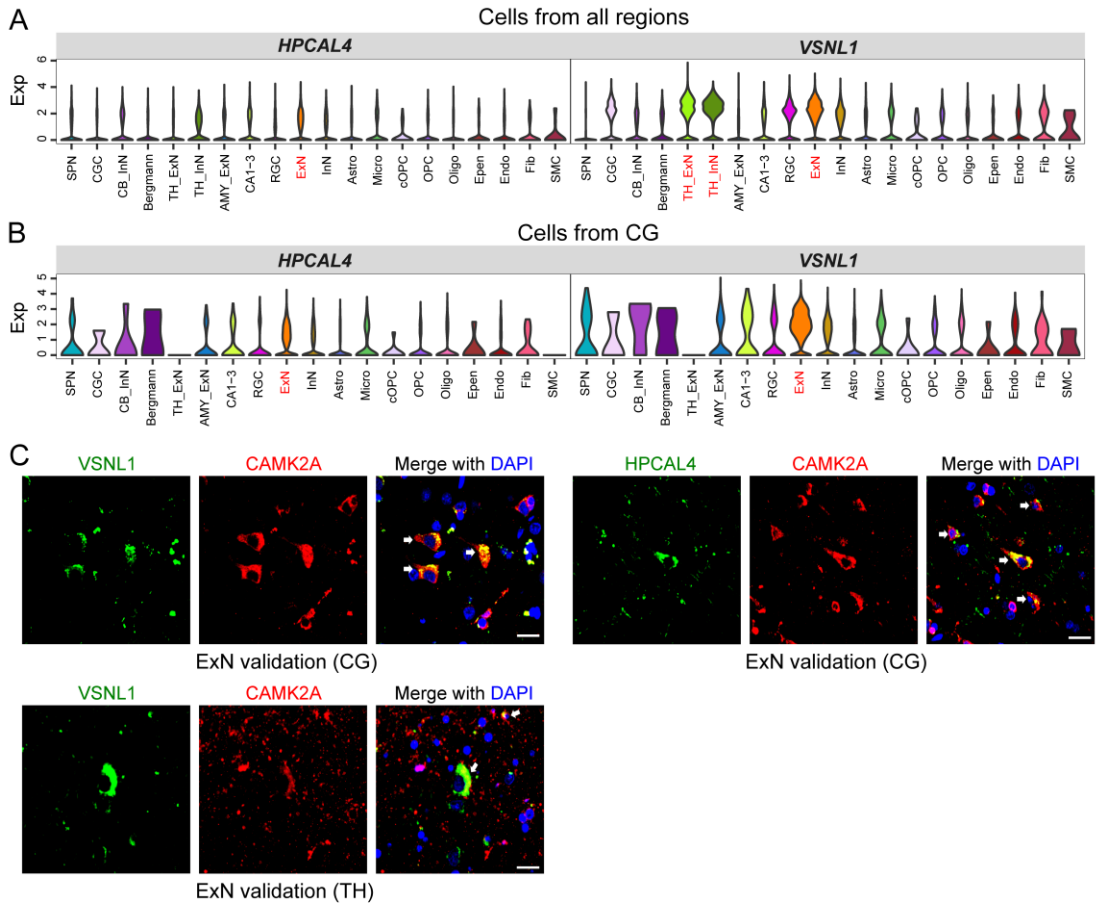

Fig. S22. Expression of *HPCAL4* and *VSNL1* across cell types. (A) Violin plot illustrates *HPCAL4* as an ExN marker and *VSNL1* as a marker of ExNs, TH-ExNs as well as TH-InNs using all cells from the ten brain regions. (B) Violin plot illustrates *HPCAL4* and *VSNL1* as ExN markers based on only cells from CG. (C) Co-expression of HPCAL4 and VSNL1 with the ExN marker CAMK2A at protein levels in CG or TH (only for VSNL1) by immunofluorescence staining. Scale bars: 20 μm.

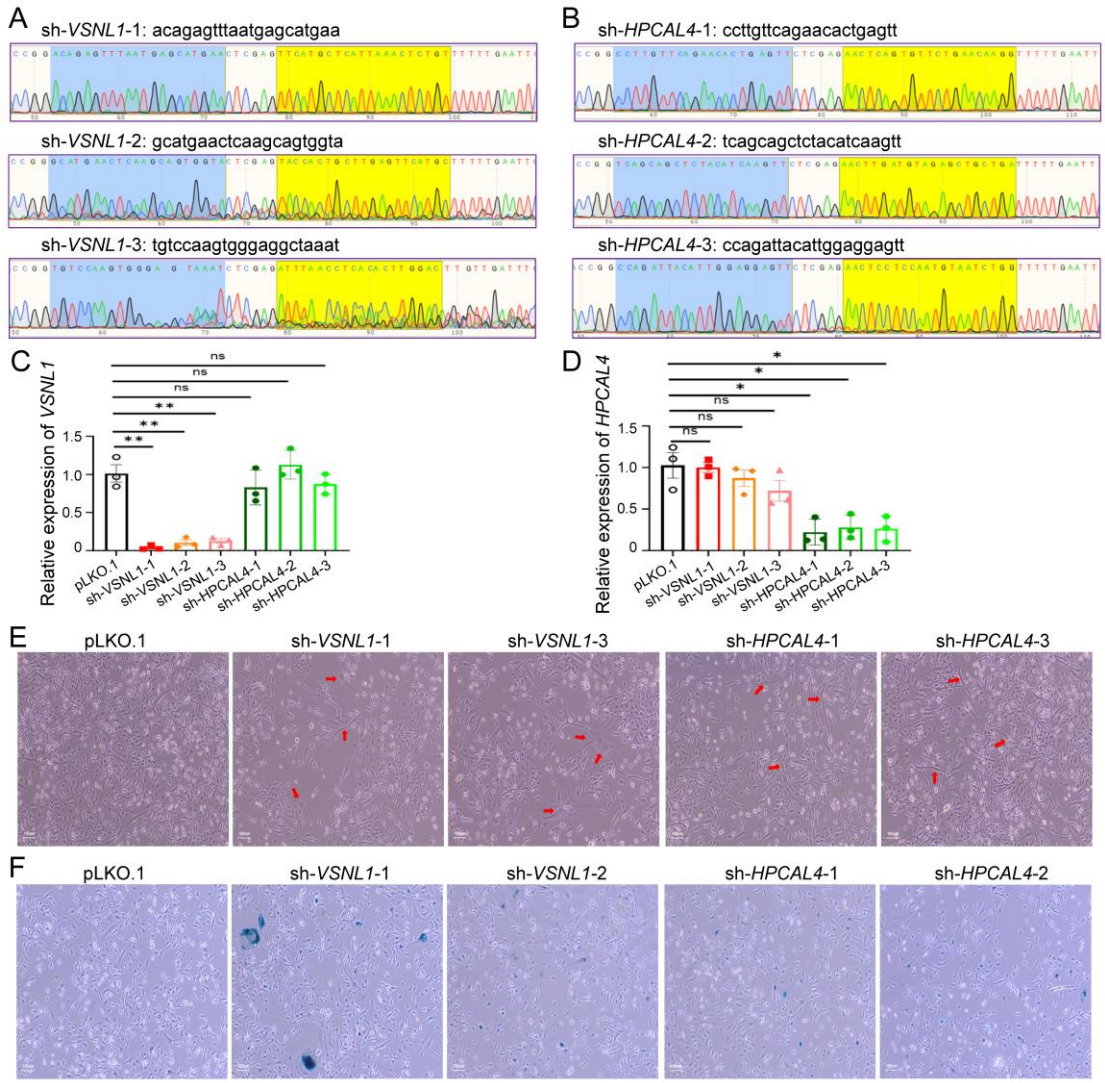

Fig. S23. Knockdown of *VSNL1* and *HPCAL4* in U251 glioma cells. (A–B) Sanger sequencing results of the corresponding short hairpin RNAs (shRNAs) used for knockdown of *VSNL1* (A) or *HPCAL4* (B). (C–D) Relative expression levels of *VSNL1* (C) or *HPCAL4* (D) based on qPCR in U251 glioma cells after each treatment of *VSNL1* or *HPCAL4* knockdown. Unpaired Student's *t*-test was used due to normal distribution and equal variances. ****: $P<0.0001$; ***: <0.001; **: $P<0.01$; *: $P<0.05$; ns: $P>0.05$. (E) The growth state of U251 glioma cells transduced with pLKO.1, sh-*VSNL1*-1, sh-*VSNL1*-3, sh-*HPCAL4*-1 and sh-*HPCAL4*-3 plasmids, respectively. Red arrows pointed cells that increased in size. (F) The senescence-associated beta-galactosidase (SA-β-gal) positive state of U251 glioma cells transduced with pLKO.1, sh-*VSNL1*-1, sh-*VSNL1*-2, sh-*HPCAL4*-1 and sh-*HPCAL4*-2 plasmids, respectively.

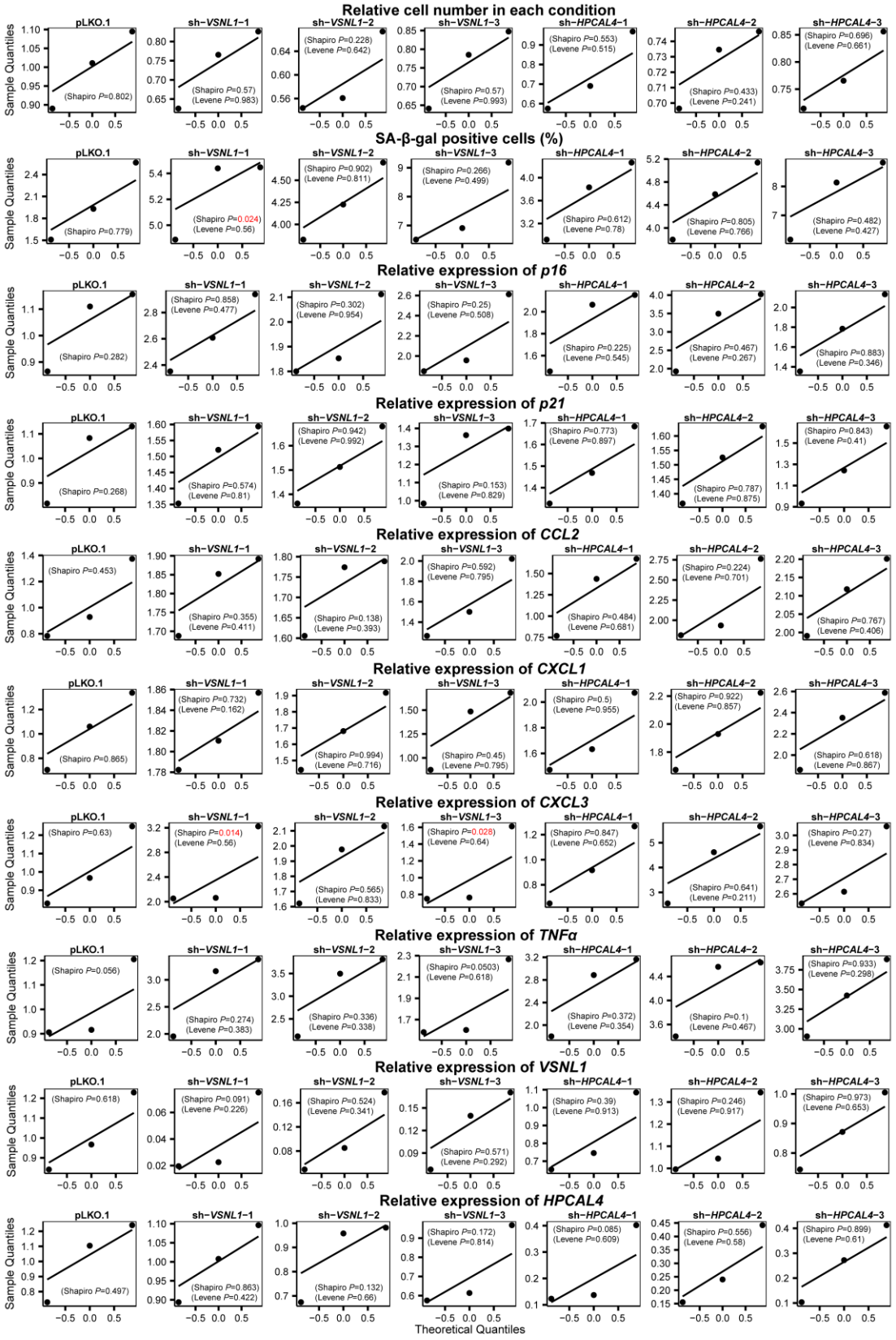

Fig. S24. Examination of data distributions after knockdown of *VSNL1* or *HPCAL4* in U251 glioma cells. First to seventh panels from left to right: Q-Q plots of raw values versus theoretical values for normality with Shapiro-Wilk and Levene's test *P* values being shown and marked by red if <0.05 in each condition, respectively.

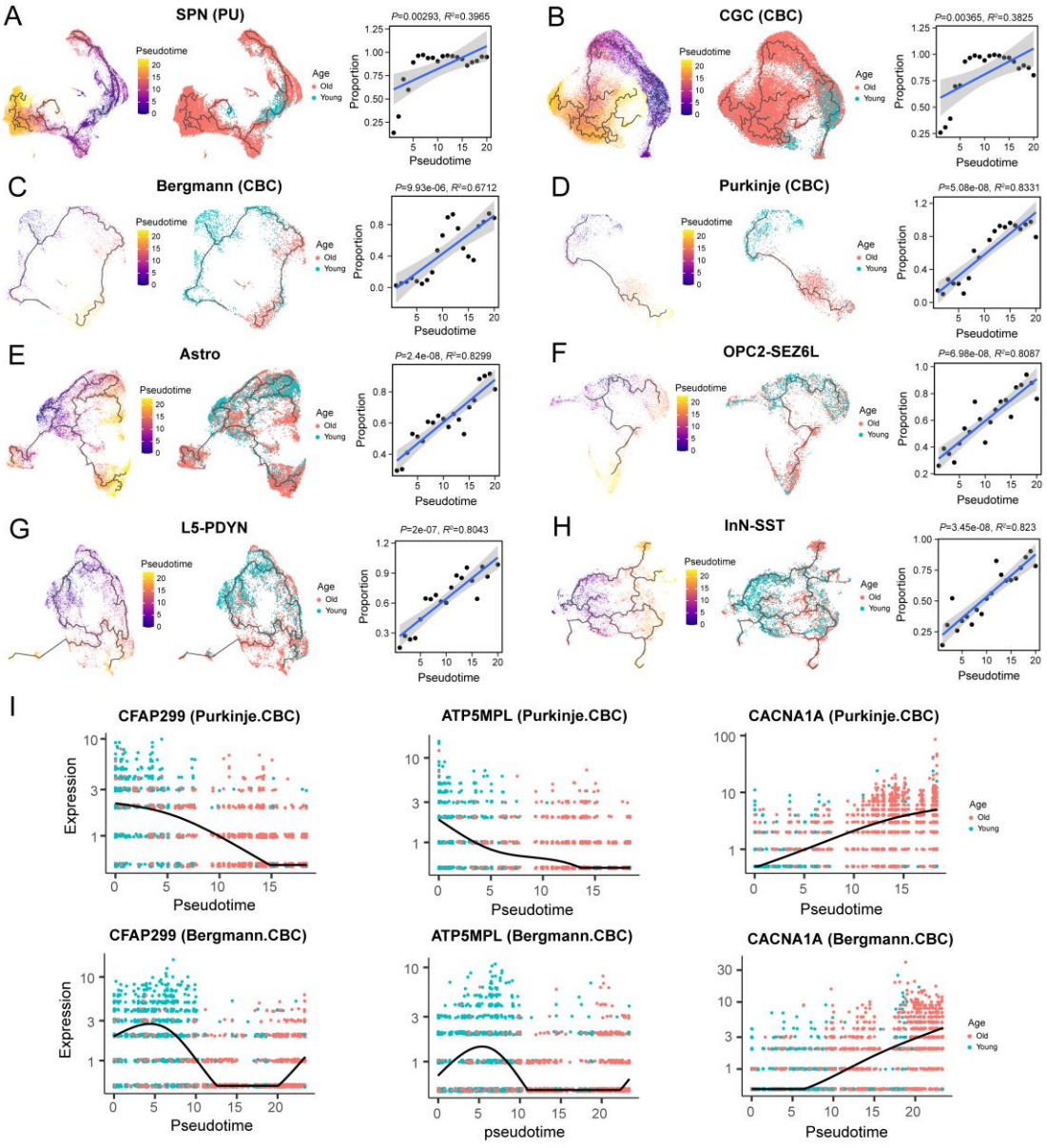

Fig. S25. Inferred progressive aging trajectories across cell types or subtypes using monocle3. (A–H) Pseudotemporal trajectories from young towards to aged nuclei of SPNs in PU (A), CGCs in CBC (B), Bergmanns in CBC (C), Purkinje neurons in CBC (D), Astros (E), glial subtype OPC2-SEZ6L (F), excitatory subtype L5-PDYN (G), and inhibitory subtype InN-SST (H). Nuclei were colored by pseudotime and age. Scatter plots presented proportions of aged nuclei along the pseudotime timeline cut into 20 time bins. *P* and R^2 values were obtained using the "lm" and "summary" functions in R. (I) Expression of age-related DEGs (i.e., *CFAP299*, *ATP5MPL*, and *CACNA1A*) across pseudotime timeline in Purkinje neurons and Bergmanns from CBC.

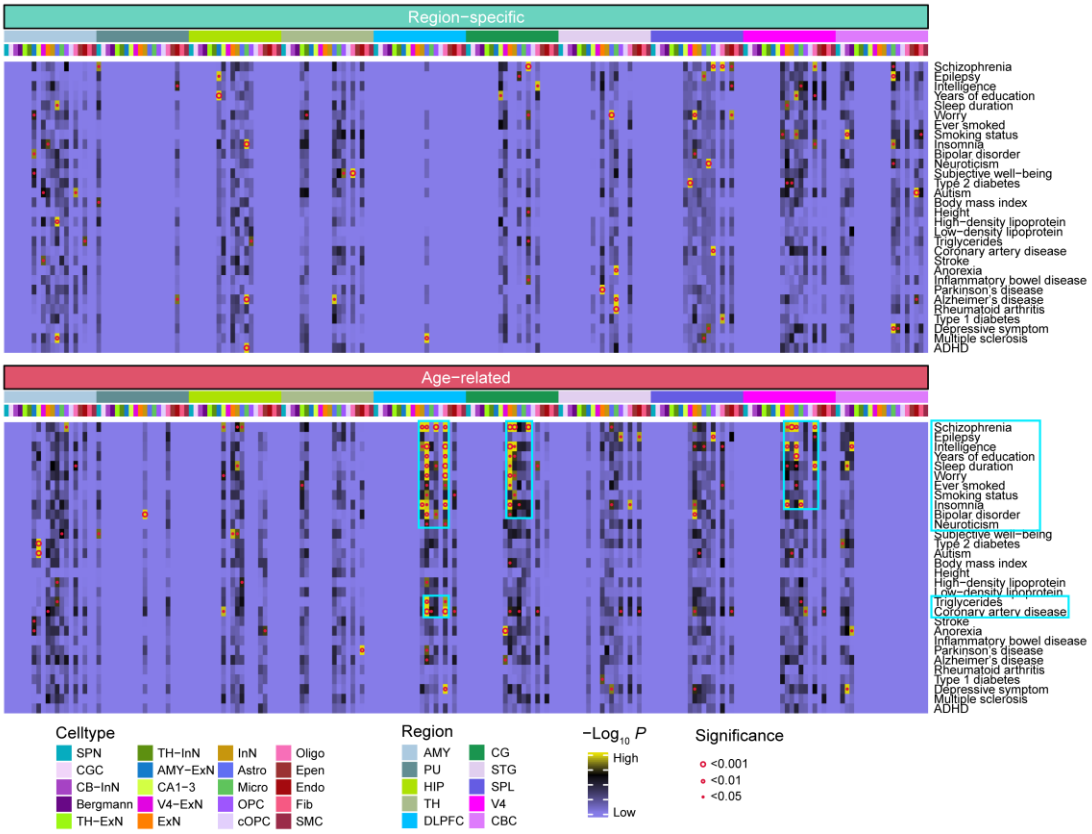

Fig. S26. Heritability enrichment of human traits/diseases across signatures related to regions and aging. Detailed description was presented in Fig. 6.